Electronic structure of FeSe monolayer superconductors

I.A. Nekrasov[1], N.S. Pavlov[1], M.V. Sadovskii[1,2], and A.A. Slobodchikov[1]

[1]*Institute for Electrophysics, Russian Academy of Sciences, Ural Branch*
106 Amundsen str., Ekaterinburg 620016, Russia
E-mail: nekrasov@iep.uran.ru

[2]*M.N. Mikheev Institute for Metal Physics, Russian Academy of Sciences, Ural Branch*
18 S. Kovalevsky str., Ekaterinburg 620290, Russia

We review a variety of theoretical and experimental results concerning electronic band structure of superconducting materials based on FeSe monolayers. Three type of systems are analyzed: intercalated FeSe systems $A_xFe_2Se_{2-x}S_x$ and $[Li_{1-x}Fe_xOH]FeSe$ as well as the single FeSe layer films on $SrTiO_3$ substrate. We present the results of detailed first principle electronic band structure calculations for these systems together with comparison with some experimental ARPES data. The electronic structure of these systems is rather different from that of typical FeAs superconductors, which is quite significant for possible microscopic mechanism of superconductivity. This is reflected in the absence of hole pockets of the Fermi surface at Γ-point in Brillouin zone, so that there are no "nesting" properties of different Fermi surface pockets. LDA+DMFT calculations show that correlation effects on Fe-$3d$ states in the single FeSe layer are not that strong as in most of FeAs systems. As a result, at present there is no theoretical understanding of the formation of rather "shallow" electronic bands at M-points. LDA calculations show that the main difference in electronic structure of FeSe monolayer on $SrTiO_3$ substrate from isolated FeSe layer is the presence of the band of O-$2p$ surface states of TiO_2 layer on the Fermi level together with Fe-$3d$ states, which may be important for understanding the enhanced T_c values in this system. We briefly discuss the implications of our results for microscopic models of superconductivity.

1. Introduction

The discovery of a new class of superconductors based on iron pnictides has opened up the new prospects for the study of high-temperature superconductivity (cf. reviews [1–6]). The nature of superconductivity in these novel materials and other physical properties significantly differs from those of high-T_c cuprates, though they still have many common features, which gives hope for a better understanding of the problem of high-temperature superconductivity in general.

The discovery of superconductivity in iron pnictides was soon followed by its discovery in iron chalcogenide FeSe. A lot of attention was attracted to this system because of its simplicity, though its superconducting characteristics (under normal conditions) were quite modest ($T_c \sim 8$ K) and its electronic structure was quite similar to that of iron pnictides (cf. review [7]).

The situation with iron chalcogenides fundamentally changed with the appearance of intercalated FeSe-based systems with the value of $T_c \sim 30$–40 K, which immediately attracted attention due to their unusual electronic structure [8,9]. Currently quite the number of such compounds is known. The first systems of this kind were $A_xFe_{2-y}Se_2$ (A = K, Rb, Cs) with the value of $T_c \sim 30$ K [10,11]. It is generally believed that superconductivity in this system appears in an ideal 122-type structure. However samples studied so far always have been multiphase, consisting of a mixture of mesoscopic superconducting and insulating (antiferromagnetic) structures such as $K_2Fe_4Se_5$, which complicates the studies of this system.

A substantial further increase of T_c up to 45 K has been achieved by intercalation of FeSe layers with rather large molecules in compounds such as $Li_x(C_2H_8N_2)Fe_{2-y}Se_2$ [12] and $Li_x(NH_2)_y(NH_3)_{1-y}Fe_2Se_2$ [13]. The growth of T_c

in these systems might be associated with increase of the distance between the FeSe layers from 5.5 Å to ∼7 Å in A_xFe$_{2-y}$Se$_2$ and 8–11 Å in the large molecules intercalated systems, i.e., with the growth of the two-dimensional character of the materials. Most recently the active studies has started of [Li$_{1-x}$Fe$_x$OH]FeSe system with the value of $T_c \sim 43$ K [38,39], where a good enough single-phase samples and single crystals were obtained.

A significant breakthrough in the study of iron-based superconductors happened with the observation of a record high T_c in epitaxial films of single FeSe monolayer on a substrate of SrTiO$_3$ (STO) [14]. These films were grown as described in Ref. 14 and most of the works to follow on the 001 plane of the STO. The tunnel experiments reported in Ref. 14 produced the record values of the energy gap, while the resistivity measurements gave the temperature of the beginning of superconducting transition substantially higher than 50 K. It should be noted that the films under study are very unstable on the air. Thus in most works the resistive transitions were mainly studied on films covered with amorphous Si or several FeTe layers. It significantly reduces the observed values of T_c. Unique measurements of FeSe films on STO, done in Ref. 15 in situ, gave the record value of $T_c > 100$ K. So far, these results have not been confirmed by the other authors. However ARPES measurements of the temperature dependence of the superconducting gap in such films, now confidently demonstrate value of T_c in the range of 65–75 K.

Films consisting of several FeSe layers produce the values of T_c significantly lower than those for the single-layer films [16]. Recently monolayer FeSe film on 110 STO plane [17] covered with several FeTe layers was grown. Resistivity measurements on these films (including measurements of the upper critical magnetic field H_{c2}) gave value of $T_c \sim 30$ K. At the same time, the FeSe film, grown on BaTiO$_3$ (BTO) substrate, doped with Nb (with even larger than in STO values of the lattice constant ∼ 3.99 Å), showed in the ARPES measurements the value of $T_c \sim 70$ K [18]. In a recent paper [19] it was reported the observation of quite high values of the superconducting gap in FeSe (from tunnelling spectroscopy) for FeSe monolayers grown on 001 plane of TiO$_2$ (anatase), which in its turn was grown on the 001 plane of SrTiO$_3$. The lattice constant of anatase is very close to the lattice constant of bulk FeSe, so FeSe film remains essentially unstretched.

Single-layer FeSe films were also grown on the graphene substrate, but the value of T_c was of the order of 8–10 K similar to bulk FeSe [20]. That emphasizes the role of the unique properties of substrates such as Sr(Ba)TiO$_3$, which can play determining role in the significant increase of T_c.

More information about the experiments on single-layer FeSe films can be found in the recently published review of Ref. 21. Below we shall concentrate on the present day understanding of the electronic structure of FeSe monolayer systems.

2. Crystal structures of iron-based superconductors

Bulk FeSe system has the simplest crystal structure among other iron high-T_c superconductors. A unit cell is a tetrahedron with Fe ion in the center and Se in its vertices. The symmetry group is $P4/nmm$ with lattice constants $a = 3.765$ Å (Fe–Fe distance) and $c = 5.518$ Å (interlayer distance), with the height of the Se ions over the Fe planes $z_{Se} = 0.2343$ Å [22].

Figure 1 schematically shows a simple crystal structure of iron-based superconductors [1–7]. The common element for all of them is the presence of the FeAs or FeSe plane (layer), where Fe ions form a simple square lattice. The pnictogen (Pn–As) or chalcogen (Ch–Se) ions are located at the centers of the squares above and below Fe plane in a staggered order. The $3d$ states of Fe in FePn plane (Ch) play a decisive role in the formation of the electronic properties of these systems, including superconductivity. In this sense, these layers are quite similar to the CuO$_2$ planes in cuprates (copper oxides). Also these systems can be considered, to a first approximation, as a quasi-two dimensional.

Note that all of the FeAs crystal structures shown in Fig. 1 are ion-covalent crystals. Chemical formula, say for a typical system 122, can be written for example as Ba^{+2}(Fe^{+2})$_2$(As^{-3})$_2$. Charged FeAs layers are held by Coulomb forces from the surrounding ions. In the bulk FeSe electrically neutral FeSe layers are held by much weaker van der Waals interactions. This makes the system suitable for intercalation of various atoms and molecules that can be fairly easy introduced between the layers of FeSe. Chemistry of intercalation processes for iron chalcogenide superconductors is discussed in detail in a recent review [23]. The crystal structure of K$_x$Fe$_2$Se$_2$ and [Li$_{1-x}$Fe$_x$OH]FeSe systems are shown in Fig. 2(b).
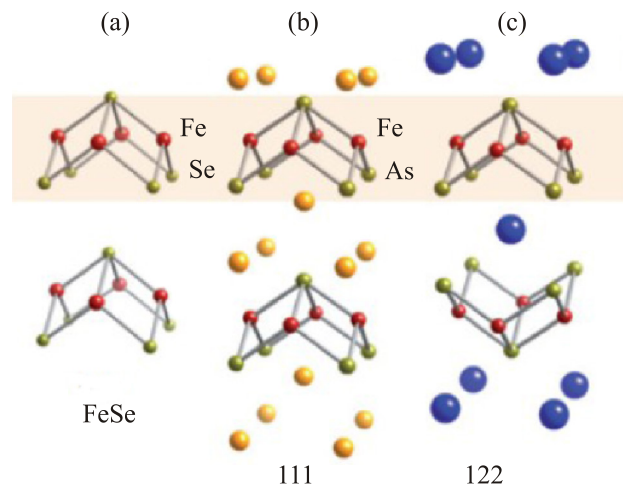

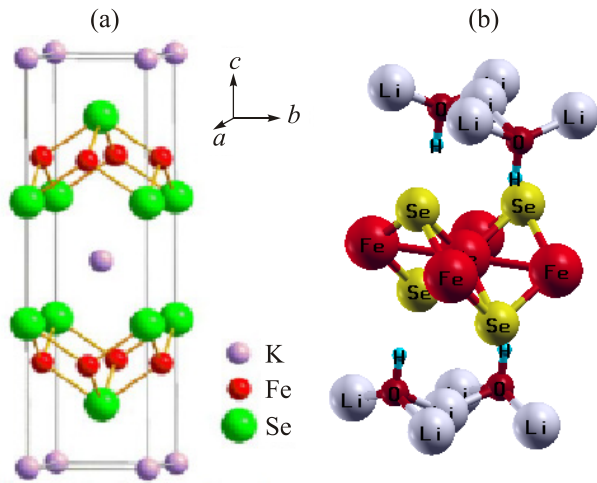*Fig. 1.* (Color online) Typical crystal structures of iron-based superconductors.

Fig. 2. (Color online) (a) Ideal ($x = 1$) crystal structure of 122-type of $K_xFe_2Se_2$, (b) Ideal ($x = 0$) crystal structure of $[Li_{1-x}Fe_xOH]FeSe$ compound.
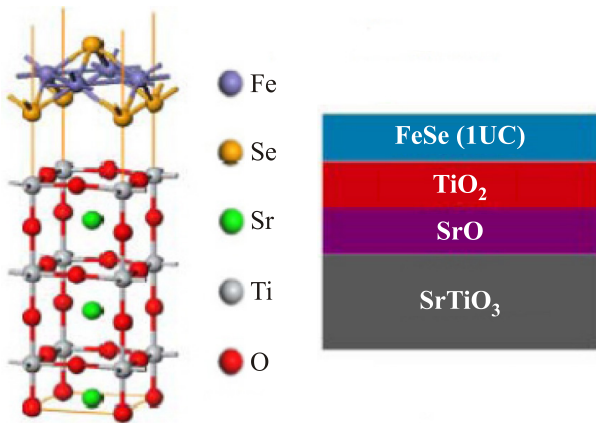

Fig. 3. (Color online) Crystal structure of FeSe monolayer on (001) surface of $SrTiO_3$.

The structure of the FeSe monolayer film on STO is shown in Fig. 3. It can be seen that the FeSe layer is directly adjacent to the surface TiO_2 layer of STO. Note that the lattice constant within FeSe layer in a bulk samples is equal to 3.77 Å, while STO has substantially greater lattice constant equal to 3.905 Å. Thus the single-layer FeSe film should be noticeably stretched, compared with the bulk FeSe. However this tension quickly disappears as the number of subsequent layers grows.

3. Electronic structure of iron–selenium systems

Electronic spectrum of iron pnictides now is well understood, both by theoretical calculations based on the modern band structure theory and ARPES experiments [1–6]. Almost all physical effects of interest to superconductivity are determined by electronic states of FeAs plane (layer), shown in Fig. 1(b). The spectrum of carriers in the vicinity of the Fermi level ± 0.5 eV, where superconductivity is formed, practically have only Fe-3d character. Thus the Fermi level is crossed by four or five bands (two or three hole and two electronic ones), forming a typical semimetallic dispersions.

In this rather narrow energy interval around the Fermi level the dispersions can be considered as parabolic [4,24]. LDA+DMFT calculations [25,26] show that the role of electronic correlations in iron pnictides, unlike the cuprates, is relatively insignificant. It is reduced to a noticeable renormalization of the effective masses of the electron and hole dispersions, as well as to general "compression" (reduction) of the bandwidth.

The presence of the electron and hole Fermi surfaces of similar size, satisfying (approximately!) the "nesting" condition plays a very important role in the theories of superconducting pairing in iron arsenides based on (antiferromagnetic) spin fluctuations [4]. We shall see below that the electronic spectrum and Fermi surfaces in the Fe chalcogenides are very different from this qualitative picture of Fe
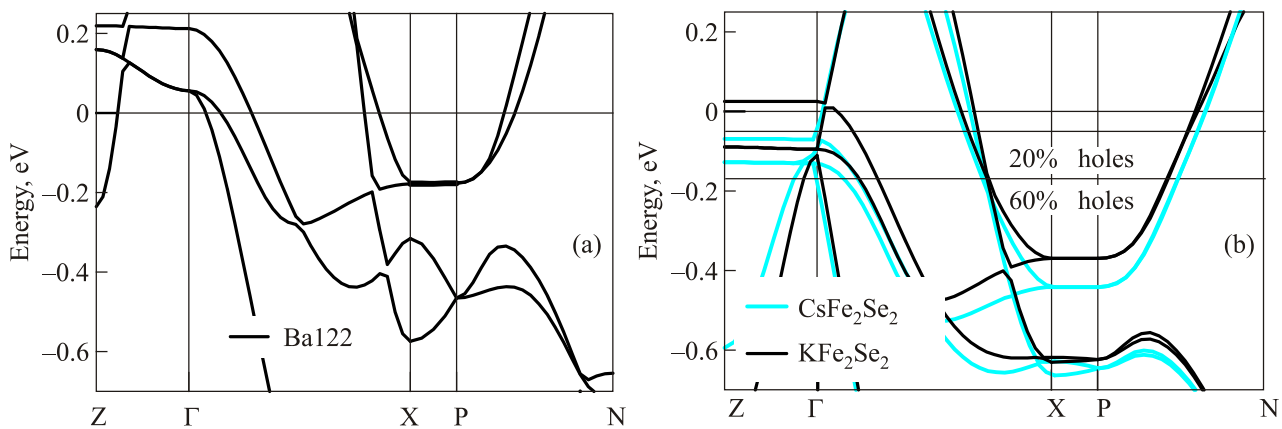

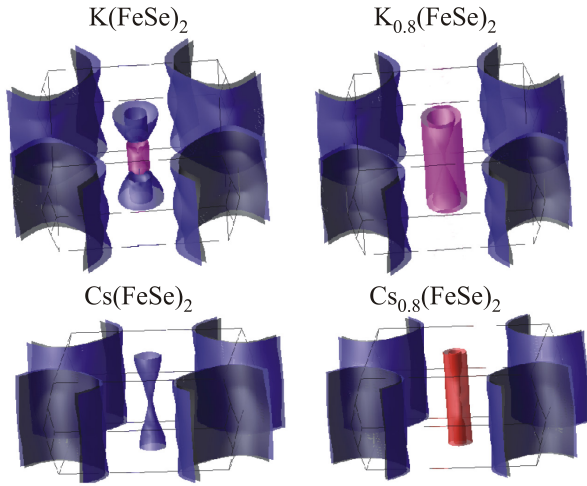*Fig. 4.* (Color online) (a) LDA bands of Ba122 near the Fermi level ($E = 0$) [29], (b) LDA bands of $K_xFe_2Se_2$ (black lines) and $Cs_xFe_2Se_2$ (blue lines). Additional horizontal lines correspond to Fermi levels of 20% and 60% hole doping [27].

Fig. 5. (Color online) LDA Fermi surfaces $A_xFe_2Se_2$ (A = K, Cs) for the stoichiometric (left) and 20% (right) hole doping [27].

pnictides. It raises the new problems for the explanations of microscopic mechanism of superconductivity in FeSe systems.

3.1. $A_xFe_2Se_2$ system

LDA calculations of electronic structure of the $A_xFe_{2-y}Se_2$ (A = K, Cs) system were performed immediately after its experimental discovery [27,28]. Surprisingly enough, this spectrum has appeared to be qualitatively different from that of the bulk FeSe and spectra of all known systems based on FeAs. In Fig. 4 we compare energy bands of $BaFe_2As_2$ (Ba122) [29] (the typical prototype of FeAs systems) and $A_xFe_{2-y}Se_2$ (A = K, Cs) [27]. One can see a significant difference in the spectra near the Fermi level.

In Fig. 5 we show the calculated Fermi surfaces for two systems $A_xFe_{2-y}Se_2$ (A = K, Cs) at various doping levels [27]. We see that they differ significantly from the Fermi surfaces of FeAs systems Fermi surfaces — in the center of the

Brillouin zone, there are only small (mainly electronic!) Fermi sheets, while the electronic cylinders in the Brillouin zone corners are substantially larger. The shape of the Fermi surface, typical for bulk FeSe and FeAs systems, can be reproduced only at a much larger (experimentally inaccessible) levels of the hole doping [27].

This shape of the Fermi surfaces in $A_xFe_{2-y}Se_2$ systems was rather soon supported by ARPES experiments. For example, in Fig. 6 we show ARPES data of Ref. 30, which obviously is in agreement with LDA data of Refs. 27, 28.

One can clearly see that in this system it is impossible to speak of any, even approximate, "nesting" properties of electron and hole Fermi surfaces.

LDA+DMFT calculations for system for various doping levels were done in Refs. 31, 32. There, along with the standard LDA+DMFT approach, we also used our LDA′+DMFT [33,34] approach, which allows, in our opinion, to solve the problem of "double counting" of Coulomb interaction in the LDA+DMFT in a more consistent way. For DMFT calculations Coulomb and exchange interactions of the electrons in the Fe-3d shell we have chosen $U = 3.75$ eV and $J = 0.56$ eV and as an impurity solver Hirsh–Fye Quantum Monte-Carlo algorithm (QMC) was used. The results of the LDA calculations are useful to compare with the ARPES data obtained in Refs. 35, 36.

It is turned out that for $K_{1-x}Fe_{2-y}Se_2$ correlation effects play quite an important role. They lead to a noticeable change in LDA energy dispersions. In contrast to iron arsenides, where the quasiparticle bands near the Fermi level are well defined, in the $K_{1-x}Fe_{2-y}Se_2$ compounds in the vicinity of the Fermi level there is a strong suppression of quasiparticle bands. This reflects the fact that the correlation effects in this system are stronger than in iron arsenides. The value of the quasiparticle renormalization (correlation narrowing) of the bands at the Fermi level is 4–5, whereas in iron arsenides this factor is only 2–3 for the same values of the interaction parameters.
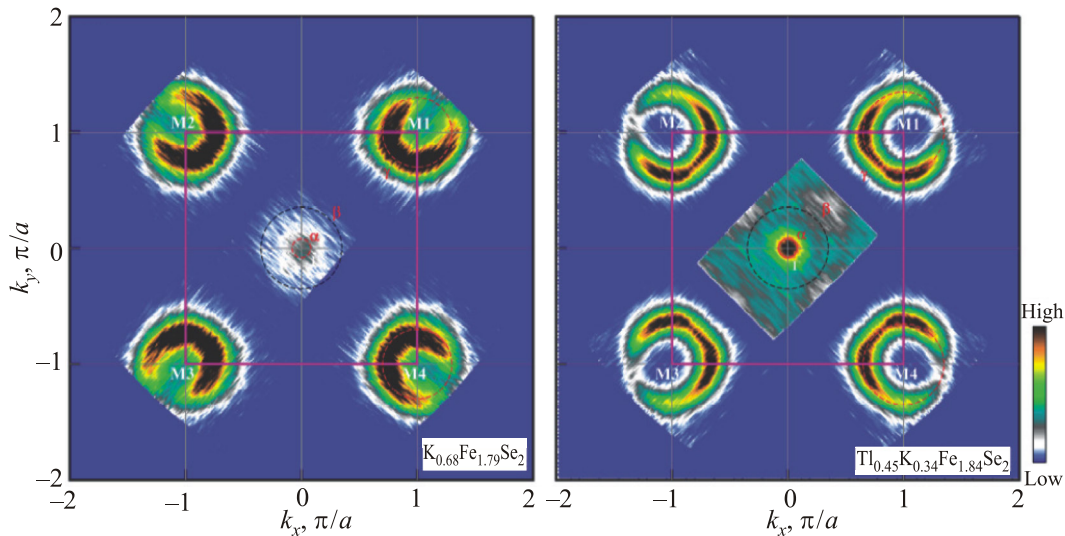

Fig. 6. (Color online) ARPES Fermi surfaces of $K_{0.68}Fe_{1.79}Se_2$ ($T_c = 32$ K) and $Tl_{0.45}K_{0.34}Fe_{1.84}Se_2$ ($T_c = 28$ K) [30].

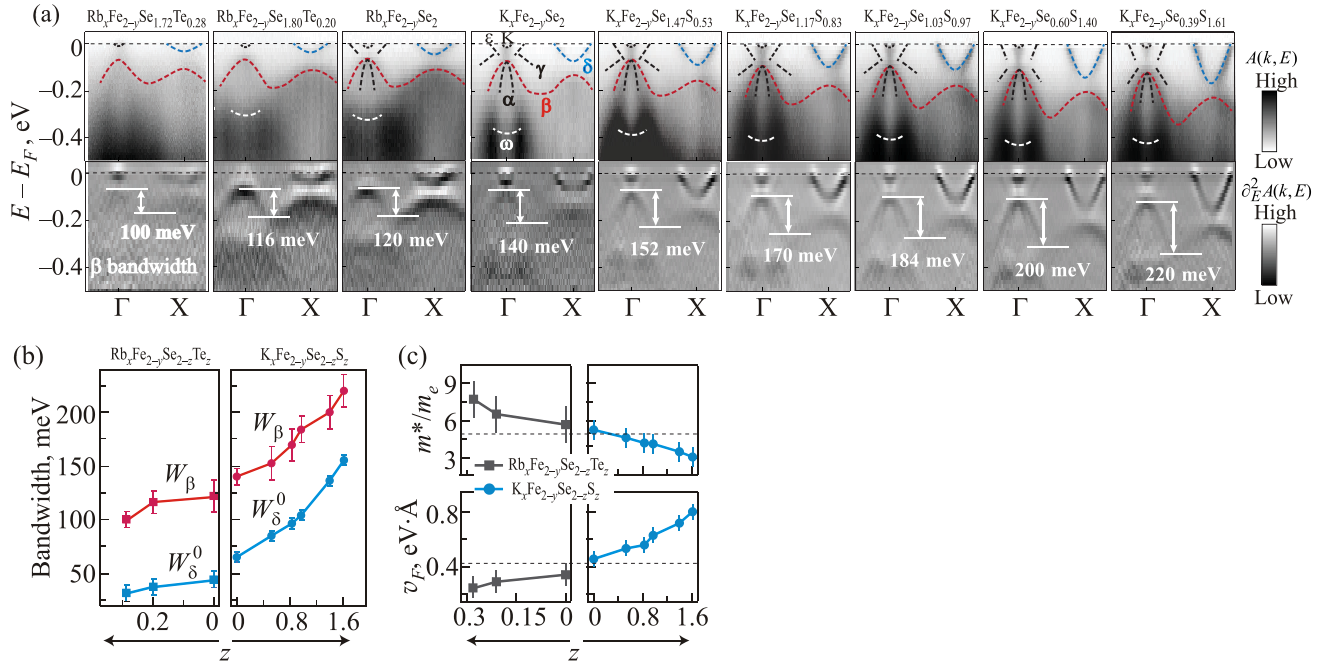*Fig. 7.* (Color online) (a) Doping dependence of the ARPES along the $\Gamma - X$ direction in $K_xFe_{2-y}Se_{2-z}S_z$. (b) The bandwidth of δ and β bands as a function of doping. (c) Doping dependence of the effective mass (m^*) and Fermi velocity (v_F) of the δ band [36].

The results of these calculations, in general, are in good qualitative agreement with the ARPES data [35,36]. Both demonstrate strong damping of quasiparticles in the immediate vicinity of the Fermi level and a strong renormalization of the effective mass as compared to systems based on FeAs. However, in our calculations formation of unusually "shallow" (depth ~ 0.05 eV) electron bands near the X-point in the Brillouin zone, observed in ARPES experiments, is not visible.

In Ref. 36 the authors reported systematic ARPES study of the $K_xFe_{2-y}Se_{2-z}S_z$ system at different doping levels. It was shown that the sulfur doping level z can control the depth of the "shallow" electron band near the X-point (Fig. 7, δ band). We tried to model this situation for different compositions of $K_xFe_{2-y}Se_{2-z}S_z$, taking into account the changes of lattice constant. We considered three cases of $K_xFe_{2-y}Se_{2-z}S_2$, $K_xFe_{2-y}Se_1S_1$ and $K_xFe_{2-y}Se_{0.4}S_{1.6}$. The appropriate values of lattice constants used in our calculations are listed in Table 1.

The LDA calculated density of states and band dispersions are presented in Figs. 8 and 9, correspondingly. Upon sulfur doping the bandwidth of Fe-3d states increases, while the bottom of the δ band slightly goes down. Corre-

sponding δ band bottom positions are 0.37, 0.38, 0.40 eV. The Se-4p states also go down in energy (see Table 1). These results are in qualitative agreement with ARPES experiments, though the unusually low values of band bottom energies ("shallow" band formation) of δ band remain a mystery. We can also note, that according to Table 1 $K_2Fe_2Se_2$ has the smallest (LDA) bandwidth of 3d states and it grows with sulfur doping. Thus one can expect, that $K_2Fe_2Se_2$ is the most correlated system in this series.

3.2. [Li$_{1-x}$Fe$_x$OH]FeSe *system*

In Ref. 42 we presented the results of LDA calculations for stoichiometric LiOHFeSe. Corresponding energy band dispersions are shown in Fig. 10(a). At first glance, the energy spectrum of this system is quite similar to the spectra of the most of FeAs-based systems and bulk FeSe. In particular, the main contribution to the density of states in the wide energy range around the Fermi level is determined solely by Fe-3d. The Fermi surfaces are qualitatively similar to that of majority of Fe-based superconductors. However, this is somewhat misleading impression. Real [Li$_{0.8}$Fe$_{0.2}$OH]FeSe system, where superconductivity was

Table 1. Lattice constants for $K_xFe_{2-y}Se_{2-z}S_z$ [27,37], LDA bandwidth of Fe-3d bands (eV) and energy interval of Se-4p states

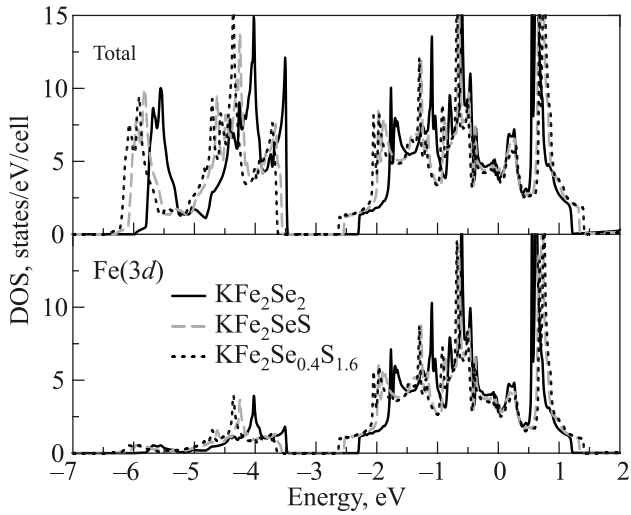| $K_xFe_{2-y}Se_{2-z}S_z$	a, Å	c, Å	Bandwidth of Fe-3d states, eV	Selenium states energies, eV
KFe$_2$Se$_2$	3.9136	14.0367	3.5	(−5.8; −3.45)
K$_{0.70}$Fe$_{1.55}$Se$_{1.01}$S$_{0.99}$	3.805	13.903	3.9	(−6.1;−3.55)
K$_{0.80}$Fe$_{1.64}$Se$_{0.42}$S$_{1.58}$	3.781	13.707	4.0	(−6.2;−3.6)

Fig. 8. LDA density of states of $K_xFe_{2-y}Se_{2-z}S_z$ compounds.

discovered, the partial replacement of Li by Fe in LiOH intercalation layers leads to noticeable LiOH electron doping, so that the Fermi energy moves upwards (relative to the stoichiometric case) by about 0.15–0.2 eV. Then, as can be seen from Fig. 10(a), the hole bands close to the

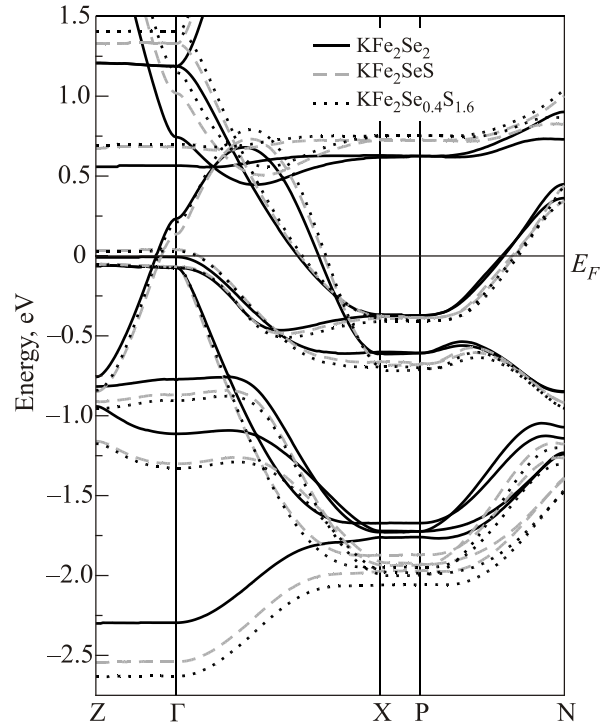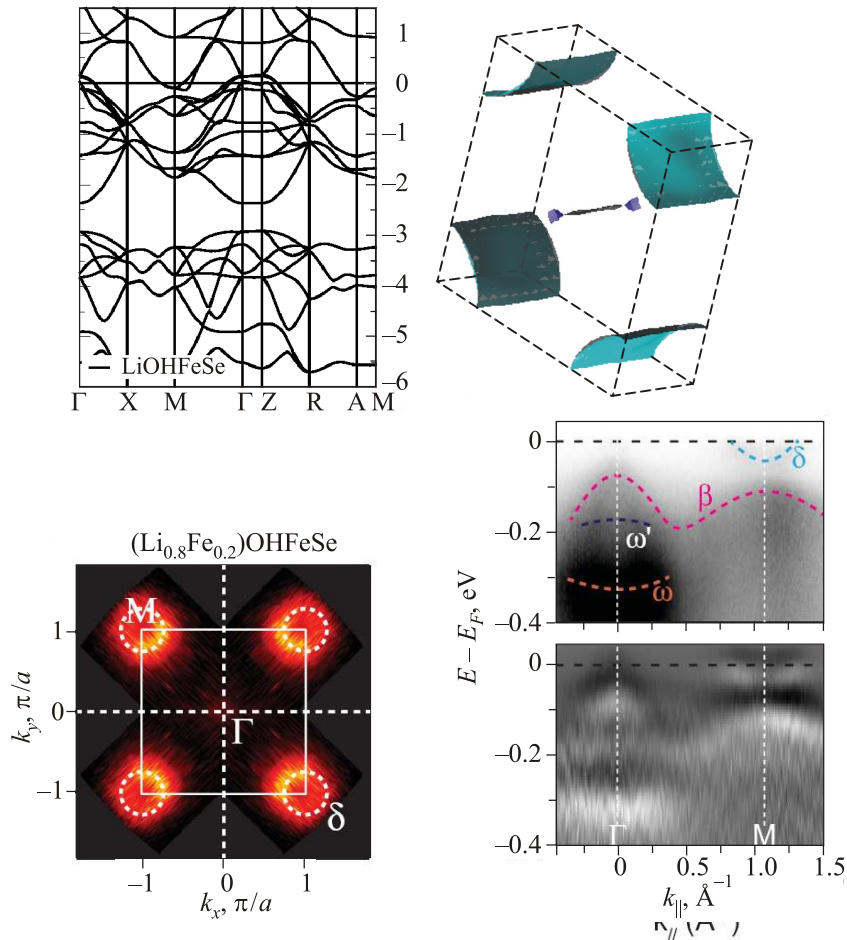*Fig. 9*. LDA band dispersions of $K_xFe_{2-y}Se_{2-z}S_z$ compounds.

Fig. 10. (Color online) (a) LDA bands for LiOHFeSe (Fermi level is at $E = 0$) [42], (b) LDA Fermi surface LiOHFeSe, corresponding to electron doping of 0.3 electrons per unit cell, (c) experimental ARPES Fermi surfaces for [$Li_{0.8}Fe_{0.2}OH$]FeSe [43], (d) experimental ARPES bands near the Fermi level of [$Li_{0.8}Fe_{0.2}OH$]FeSe [43].

Γ-point shifts below the Fermi level and the hole cylinders of Fermi surface almost disappear. The general view of the LDA calculated Fermi surface for this level of electron doping is shown in Fig. 10(b). It has an obvious similarity with the results for the $A_x Fe_{2-y} Se_2$ system (see Fig. 5). These conclusions are directly confirmed by ARPES experiments [43], with the results shown in Fig. 10 (c).

From Fig. 10 one can see that the Fermi surface consists mostly of electronic cylinders surrounding the *M*-points, while around the Γ-point the Fermi surface is either absent or very small. In any case, for this system we can not speak of any "nesting" of electron and hole Fermi surfaces in any sense. Electronic dispersions found in the ARPES experiments are very similar to corresponding ARPES dispersions reported in Refs. 35, 36 for $K_x Fe_{2-y} Se_{2-z} S_2$ system. These are qualitatively similar to dispersions obtained in LDA and LDA+DMFT calculations, including rather strong correlation bands narrowing (by about several times with different compression factor for different bands) [31,32]. However, the explanation of the formation of extremely "shallow" electron δ band with depth ∼ 0.05 eV near the *M*-point remains unclear. This requires an unusually strong correlation compression which hardly can be obtained from the LDA+DMFT calculations, while the diameter of electronic cylinders around *M*-points is nearly unchanged by correlations and almost coincides with the results of LDA calculations.

An interesting debate flared up around the possible nature of magnetic ordering of Fe ions, which replaces Li ions within intercalation LiOH layers. In Ref. 38 it was stated that this ordering is just a canted antiferromagnet. However, in Ref. 39, on the basis of magnetic measurements, it was claimed that it is ferromagnetic, with Curie temperature $T_C \sim 10$ K, i.e., substantially below the superconducting transition temperature. This conclusion was confirmed indirectly in Ref. 40 by observing the scattering of neutrons on the lattice of Abrikosov vortices, which might be induced in the FeSe layers by ferromagnetic or-

dering of Fe spins in the $Li_{1-x} Fe_x OH$ layers. At the same time, in Ref. 41 it was argued that Mössbauer measurements indicate the absence of any kind of magnetic ordering on Fe ions in intercalation layers.

In Ref. 42 LSDA calculations of the exchange integrals were performed for some typical magnetic configurations of Fe ions, replacing Li in LiOH layers. For the most likely magnetic configuration, leading to magnetic ordering, we have obtained the positive (ferromagnetic) sign of the exchange interaction, and simple estimate of the Curie temperature produced the value of Curie temperature $T_C \approx 10$ K, which is in excellent agreement with the results of experiment of Refs. 39, 40.

3.3. FeSe *monolayer films*

LDA calculations of the spectrum of the isolated FeSe monolayer can be performed in a standard slab approach. To calculate electronic properties we used the *Quantum-Espresso* [44] package. The results of these calculations are shown in Fig. 11(a). It can be seen that the spectrum has the form typical for FeAs-based systems and bulk FeSe discussed in detail above. However ARPES experiments [45–47] convincingly show that this is not so. For FeSe monolayers on STO only electronic Fermi surface sheets are observed around the *M*-points of the Brillouin zone, while hole sheets, centered around the Γ-point (in the center of the zone), are simply absent. An example of such data is shown in Fig. 12(a) [45]. Similarly to intercalated FeSe systems there are no signs of "nesting" of Fermi surface — there are just no surfaces to "nest"!

In an attempt to explain the contradiction between ARPES experiments [45] and band structure calculations reflected in the absence of hole cylinder in the Γ-point, one can suppose that this may be the consequence of FeSe/STO monolayer stretching due to mismatch of lattice constants of the bulk FeSe and STO. We have studied this problem by varying the lattice parameter *a* and Se height z_{Se} in the range ±5% around the bulk FeSe parameters.
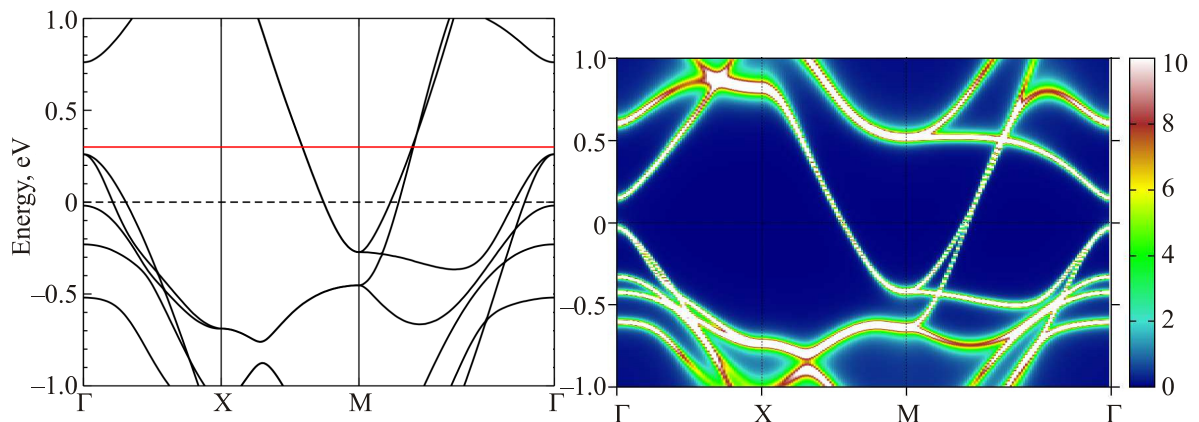

Fig. 11. (Color online) (a) LDA bands of an isolated FeSe monolayer near the Fermi level (*E* = 0). Red line shows approximate Fermi level position to agree with ARPES experimental data. (b) LDA+DMFT bands of isolated electronically doped FeSe monolayer near the doping-shifted Fermi level.
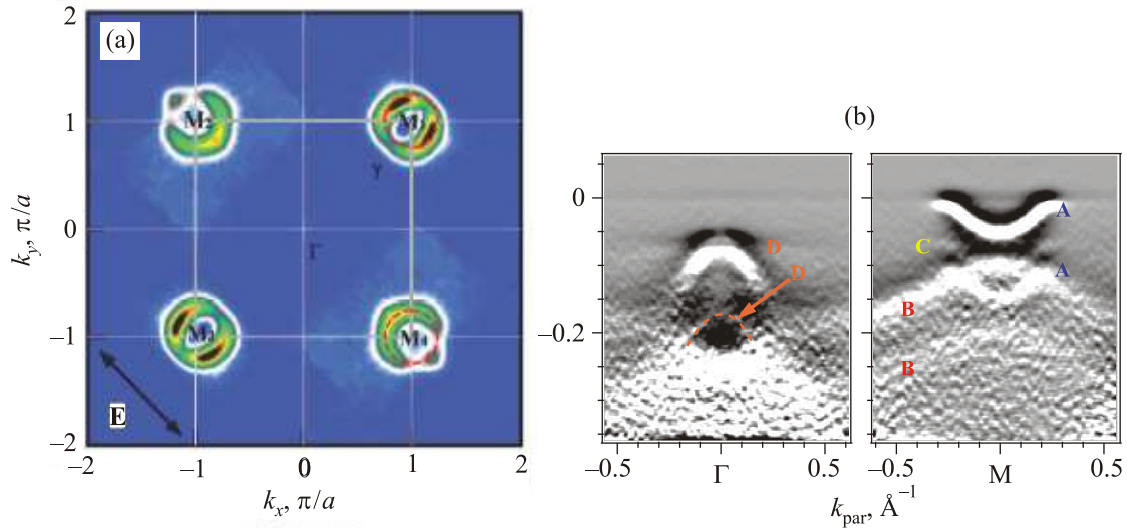
Fig. 12. (Color online) (a) Experimental ARPES Fermi surface of FeSe monolayer [45], (b) experimental ARPES bands of FeSe monolayer near the Fermi level [46].

Before the electronic structure was calculated crystal structure was relaxed. Unfortunately, the conclusion was that the changes of lattice parameters do not lead to qualitative changes of FeSe Fermi surfaces and the hole cylinders in the Γ-point always remain.

However, there is another rather simple qualitative explanation for the absence of hole cylinders and the observed Fermi surfaces can be obtained by assuming that the system is just electronically doped. The Fermi level has to be moved upwards in energy by the value of ~ 0.2–0.25 eV, as shown by the solid (red) horizontal line in Fig. 11(a), which corresponds to the doping level of 0.15–0.2 electron per Fe ion.

Strictly speaking, the nature of this doping is not fully identified. But there is a common belief that it is associated with the formation of oxygen vacancies in the $SrTiO_3$ substrate (within the topmost layer of TiO_2), occurring during the various technological steps used during the film preparation, such as annealing, etching, etc. It should be noted that the formation of the electron gas at the interface with the $SrTiO_3$ is a widely known phenomenon, which was studied for a long time [48]. At the same time, for FeSe/STO system this issue remains poorly understood (see, however, Refs. 49, 50).

Electron correlations have relatively little influence on the spectrum of the FeSe monolayer. Figure 11(b) shows the results of LDA+DMFT calculations for estimated experimental value of electron doping. DMFT calculations were done for the values of the Coulomb and exchange (Hund) electron interactions in the Fe-3d shell equal to $U = 3.5$ eV and $J = 0.85$ eV. As impurity solver we used the continuous time quantum Monte-Carlo (CT-QMC) algorithm. The inverse dimensionless temperature was taken to be $\beta = 40$. It can be seen that the spectrum is very weakly renormalized by correlations and preserves the

general LDA-like shape, with a slight band compression factor of about ~ 1.3.

Electronic dispersion in monolayer FeSe films was measured by ARPES and reported in a number of papers [18,46]. The results of Ref. 46 are shown in Fig. 12(b). They are consistent with those of other studies and, in general, are similar to those obtained for the intercalated FeSe systems (see, e.g., Fig. 10(c)). Overall, they are qualitatively similar to the results of LDA+DMFT but there is no quantitative agreement. In particular, in the ARPES experiments the presence of the unusual "shallow" electron band at M-point, with the band bottom at ~ 0.05 eV is clearly observed. However, our calculated dispersions show a "depth" of almost an order of magnitude larger.

It should also be noted that an additional "shadow" or "replica" electronic band near the M-point was observed in Ref. 46, which is ~ 100 meV below the parent band "shallow" band, and is clearly visible in Fig. 12(b). This "shadow" band is completely missed in the band structure calculations. The possible nature of this band (due to interaction with 100 meV STO optical phonons) and its importance for mechanisms of T_c enhancement in FeSe/STO films was discussed in Ref. 46.

Now let us discuss the results of our LDA calculations of electronic structure of the FeSe monolayer film on $SrTiO_3$ substrate as shown in Fig. 3. These calculations were again performed with *Quantum Espresso* [44]. By looking on left panel of Fig. 13 one can immediately recognize that there appears an additional hole band near the M-point. To understand its origin we plotted on right panel of Fig. 13 O-2p states of topmost surface TiO_2 layer of STO substrate. We can conclude, that the presence of STO interface leads to the appearance of this additional band of O-2p surface states near the Fermi level with probable "nesting" with hole Fe-3d band with nesting vector $\mathbf{Q} = 0$.
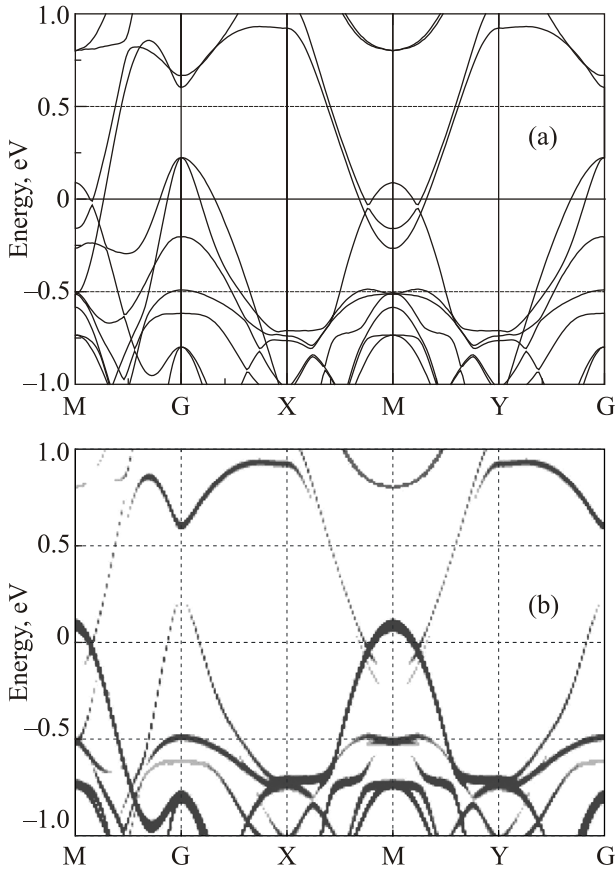
Fig. 13. (a) LDA calculated band dispersion of FeSe monolayer on SrTiO$_3$ substrate; (b) LDA calculated O-2p states of surface TiO$_2$ layer of STO substrate.

These results are essentially confirmed by the available ARPES experiments. An apparent absence of obvious "nesting" properties between electron and hole Fermi surface pockets cast serious doubts upon the most popular picture of Cooper pairing, assumed to realize in FeAs systems, based on the exchange of antiferromagnetic fluctuations and leading to the picture of $s^{\pm}$ pairing [4].

The role of electronic correlations in FeSe monolayers remain rather controversial. LDA+DMFT calculations for K$_x$Fe$_2$Se$_2$S system show that here these correlations are more important than in typical FeAs systems, leading to stronger bandwidth compression (different for different Fe-3d bands) and rather poorly defined quasiparticles close to the Fermi level. In contrast to this, in isolated FeSe single-layer system the same calculations demonstrate rather weak influence of correlations with small bandwidth compression (effective mass renormalization). The role of SrTiO$_3$ substrate may also be important leading to the appearance of O-2p hole band of TiO$_2$ layer in the vicinity of the Fermi level.

The serious problems for understanding of the observable electronic structure of FeSe monolayer systems remain to be solved. In particular, at present there are no acceptable explanation of formation of unusually "shallow" electronic bands around the $M(X)$-points, with Fermi energies ~ 0.05 eV, observed in ARPES experiments on all of these systems. It can be guessed that this fact reflects our poor understanding of electron correlations and the question remains open. Note that the existence of such small Fermi energies in conduction bands of the system under discussion signifies the serious problems related to the antiadiabatic regime of Cooper pairing [51]. Taking into account the typical values of the energy gap in FeSe monolayer superconductors $\Delta \sim 0.015–0.020$ eV [18,47] we also obtain the anomalously low gap to the Fermi energy ratios: $\Delta / E_F \sim 0.25–0.5$, which indicate, that these superconductors belong to BCS–BEC crossover region [52,53].

Also we observe rather small splitting of electron bands at M-point. The relevance of these results to ARPES experiments and their significance for enhanced superconductivity in FeSe/STO system are at present unclear. However, the additional electron band splitting may have the relation to the observation of the "replica" band at M-point [46], providing the explanation of its appearance not related to interaction with optical phonons in STO.

4. Conclusion

We have presented a short review of calculations of electronic band structure of high-T_c systems based on FeSe monolayers, from intercalated compounds like A$_x$Fe$_2$Se$_{2-z}$S$_z$ (A = K, Cs,...) and [Li$_{1-x}$Fe$_x$OH]FeSe to single FeSe layer films of SrTiO$_3$ substrate.

Our calculations show, that in all these systems the general structure of electronic spectrum is significantly different from the "standard model" typical for almost all FeAs-based superconductors and bulk FeSe. This structure is characterized by the practical absence of hole-like Fermi surface cylinders around the Γ-point at the center of the Brillouin zone with only electron-like cylinders present around the M-points in the corners of the Brillouin zone.

1. M.V. Sadovskii, *Usp. Fiz. Nauk* **178**, 1243 (2008) [*Phys. Usp.* **51**, 1201 (2008)].
2. K. Ishida, Y. Nakai, and H. Hosono, *J. Phys. Soc. Jpn.* **78**, 062001 (2009).
3. D.C. Johnson, *Adv. Phys.* **59**, 803 (2010).
4. P.J. Hirshfeld, M.M. Korshunov, and I.I. Mazin, *Rep. Prog. Phys.* **74**, 124508 (2011).
5. G.R. Stewart, *Rev. Mod. Phys.* **83**, 1589 (2011).

6. A.A. Kordyuk, *Fiz. Niz. Temp.* **38**, 1119 (2012) [*Low Temp. Phys.* **38**, 888 (2012)].

7. Y. Mizugushi and Y. Takano, *J. Phys. Soc. Jpn.* **79**, 102001 (2010).

8. M.V. Sadovskii, E.Z. Kuchinskii, and N.A. Nekrasov, *JMMM* **324**, 3481 (2010).

9. I.A. Nekrasov and M.V. Sadovskii, *Pis'ma Zh. Eksp. Teor. Fiz.* **99**, 687 (2014) [*JETP Lett.* **99**, 598 (2014)].

10. Guo Jiangang, Jin Shifeng, Wang Shunchong, Zhu Kaixing, Zhou Tingting, He Meng, and Chen Xialong, *Phys. Rev. B* **82**, 180520 (2010).

11. Y.J. Yan, A.F. Wang, J.J. Ying, Z.Y. Li, W. Qin, J.Q. Luo, J. Hu, and X.H. Chen, *Chin. Sci. Rep.* **2**, 212 (2012).

12. T. Hatakeda, T. Noji, T. Kawamata, M. Kato, and Y. Koike, *J. Phys. Soc. Jpn.* **82**, 123705 (2013).

13. M. Burrad-Lucas, D.G. Free, S.J. Sedlmaier, J.D. Wright, S.J. Cassidy, Y. Hara, A.J. Corkett, T. Lancaster, P.J. Baker, S.J. Blundell, and S.J. Clarke, *Nature Mater.* **12**, 15 (2013).

14. Qing-Yan Wang, Zhi Li, Wen-Hao Zhang, Zuo-Cheng Zhang, Jin-Song Zhang, Wei Li, Hao Ding, Yun-Bo Ou, Peng Deng, Kai Ghang, Jing Wen, Can-Li Song, Ke He, Jin-Feng Jia, Shuai-Hua Ji, Ya.-Yu. Wang, Li-Li Wang, Xi Chan, Xu-Cun Ma, and Qi-Kun Xue, *Chin. Phys. Lett.* **29**, 037402 (2012).

15. Jian-Feng Ge, Zhi-Long Liu, Chun-Lei Gao, Dong Qian, Qi-Kun Xue, Ying Liu, and Jin-Feng Jia, *Nature Mater.* **14**, 285 (2015).

16. Y. Miyata, K. Nakayama, K. Sugawara, T. Sato, and T. Takahashi, *Nature Mater.* **14**, 775 (2015).

17. Guanyu Zhou, Ding Zhang, Chong Liu, Chenjia Tang, Xiaoxiao Wang, Zheng Li, Canli Song, Shuaihua Ji, Ke He, Lili Wang, Xucun Ma, and Qi-Kun Xue, *ArXiv:1512.01948*.

18. R. Peng, H.C. Xu, S.Y. Tan, M. Xia, X.P. Shan, Z.C. Huang, C.H.P. Wen, Q. Song, T. Zhang, B.P. Xie, and D.L. Feng, *Nature Commun.* **5**, 5044 (2014).

19. Hao Ding, Yan-Feng Lv, Kun Zhao, Wen-Lin Wang, Lili Wang, Can-Li Song, Xi Chen, Xu-Cun Ma, and Qi-Kun Xue, *ArXiv:1603.00999*.

20. Can-Li Song, Yi-Lin Wang, Ye-Ping Jiang, Zhi Li, Lili Wang, Ke He, Xi Chen, Xu-Cun Ma, and Qi-Kun Xue, *Phys. Rev. B* **84**, 020503(R) (2011).

21. Xu Liu, Lin Zhao, Shaolong He, Junfeng He, Defa Liu, Daixiang Mou, Bing Shen, Yong Hu, Jianwei Huang, and X.J. Zhou, *J. Phys.: Condens. Matter* **27**, 183201 (2015).

22. Alaska Subedi, Lijun Zhang, D.J. Singh, and M.H. Du, *Phys. Rev. B* **78**, 134514 (2008).

23. H.K. Vivanco and E.E. Rodriguez, *ArXiv:1603.02334*.

24. E.Z. Kuchinskii and M.V. Sadovskii, *Pis'ma Zh. Eksp. Teor. Fiz.* **91**, 729 (2010) [*JETP Lett.* **91**, 661 (2010)].

25. S.L. Skornyakov, A.V. Efremov, N.A. Skorikov, M.A. Korotin, Yu.A. Izyumov, V.I. Anisimov, A.V. Kozhevnikov, and D. Vollhardt, *Phys. Rev. B* **80**, 092501 (2009).

26. I.A. Nekrasov, N.S. Pavlov, and M.V. Sadovskii, *Pis'ma Zh. Eksp. Teor. Fiz.* **102**, 30 (2015) [*JETP Lett.* **102**, 26 (2015)].

27. I.A. Nekrasov and M.V. Sadovskii, *Pis'ma Zh. Eksp. Teor. Fiz.* **93**, 182 (2011) [*JETP Lett.* **93**, 166 (2011)].

28. I.R. Shein and A.L. Ivanovskii, *Phys. Lett. A* **375**, 1028 (2011).

29. I.A. Nekrasov, Z.V. Pchelkina, and M.V. Sadovskii, *Pis'ma Zh. Eksp. Teor. Fiz.* **88**, 155 (2008) [*JETP Lett.* **88**, 144 (2008)].

30. L. Zhao, D. Mou, S. Liu, J. He, Y. Peng, L. Yu, X. Liu, G. Liu, S. He, X. Dong, J. Zhang, J.B. He, D.M. Wang, G.F. Chen, J.G. Guo, X.L. Chen, X. Wang, Q. Peng, Z. Wang, S. Zhang, F. Yang, Z. Xu, C. Chen, and X.J. Zhou, *Phys. Rev. B* **83**, 140508(R) (2011).

31. I.A. Nekrasov, N.S. Pavlov, and M.V. Sadovskii, *Pis'ma Zh. Eksp. Teor. Fiz.* **97**, 18 (2013) [*JETP Lett.* **97**, 15 (2013)].

32. I.A. Nekrasov, N.S. Pavlov, and M.V. Sadovskii, *Zh. Eksp. Teor. Fiz.* **144**, 1061 (2013) [*JETP* **117**, 926 (2013)].

33. I.A. Nekrasov, N.S. Pavlov, and M.V. Sadovskii, *Pis'ma Zh. Eksp. Teor. Fiz.* **95**, 659 (2012) [*JETP Lett.* **95**, 581 (2012)].

34. I.A. Nekrasov, N.S. Pavlov, and M.V. Sadovskii, *Zh. Eksp. Teor. Fiz.* **143**, 713 (2013) [*JETP* **116**, 620 (2013)].

35. M. Yi, D.H. Lu, R. Yu, S.C. Riggs, J.H. Chu, B. Lv, Z.K. Liu, M. Lu, Y.T. Cui, M. Hashimoto, S.K. Mo, Z. Hussain, C.W. Chu, I.R. Fisher, Q. Si, and Z.X. Shen, *Phys. Rev. Lett.* **110**, 067003 (2013).

36. X.H. Niu, S.D. Chen, J. Jiang, Z.R. Ye, T.L. Yu, D.F. Xu, M. Xu, Y. Feng, Y.J. Yan, B.P. Xie, J. Zhao, D.C. Gu, L.L. Sun, Q. Mao, H. Wang, M. Fang, C.J. Zhang, J.P. Hu, Z. Sun, and D.L. Feng, *Phys. Rev. B* **93**, 054516 (2016).

37. H. Lei, M. Abeykoon, E.S. Bozin, K. Wang, J.B. Warren, and C. Petrovic, *Phys. Rev. Lett.* **107**, 137002 (2011).

38. X.F. Lu, N.Z. Wang, H. Wu, Y.P. Wu, D. Zhao, X.Z. Zeng, X.G. Luo, T. Wu, W. Bao, G.H. Zhang, F.Q. Huang, Q.Z. Huang, and X.H. Chen, *Nature Mater.* **14**, 325 (2015).

39. U. Pachmayr, F. Nitsche, H. Luetkens, S. Kamusella, F. Brückner, R. Sarkar, H.-H. Klauss, and D. Johrendt, *Angew. Chem. Int. Ed.* **54**, 293 (2015).

40. J.W. Lynn, X. Zhou, C.K. H. Borg, S.R. Saha, J. Paglione, and E.E. Rodriguez, *Phys. Rev. B* **92**, 0605510(R) (2015).

41. F. Nejasattari and Z.M. Stadnik, *J. All. Comp.* **652**, 470 (2015).

42. I.A. Nekrasov and M.V. Sadovskii, *Pis'ma Zh. Eksp. Teor. Fiz.* **101**, 50 (2015).

43. X.H. Niu, R. Peng, H.C. Xu, Y.J. Yan, J. Jiang, D.F. Xu, T.L. Yu, Q. Song, Z.C. Huang, Y.X. Wang, B.P. Xie, X.F. Lu, N.Z. Wang, X.H. Chen, Z. Sun, and D.L. Feng, *Phys. Rev. B* **92**, 060504(R) (2015).

44. Paolo Giannozzi, S. Baroni, N. Bonini, M. Calandra, R. Car, C. Cavazzoni, D. Ceresoli, G.L. Chiarotti, M. Cococcioni, I. Dabo, A. Dal Corso, S. de Gironcoli, S. Fabris, G. Fratesi, R. Gebauer, U. Gerstmann, C. Gougoussis, A. Kokalj, M. Lazzeri, L. Martin-Samos, N. Marzari, F. Mauri, R. Mazzarello, S. Paolini, A. Pasquarello, L. Paulatto, C. Sbraccia, S. Scandolo, G. Sclauzero, A.P. Seitsonen, A. Smogunov, P. Umari, and R.M. Wentzcovitch, *J. Phys.: Condens. Matter* **21**, 395502 (2009).

45. Defa Liu, Wenhao Zhang, Daixiang Mou, Junfeng He, Yun-Bo Ou, Qing-Yan Wang, Zhi Li, Lili Wang, Lin Zhao, Shaolong He, Yingying Peng, Xu Liu, Chaoyu Chen, Li Yu, Guodong Liu, Xiaoli Dong, Jun Zhang, Chuangtian Chen,

Zuyan Xu, Jiangping Hu, Xi Chen, Xucun Ma, Qikun Xue, and X.J. Zhou, *Nature Commun.* **3**, 931 (2012).

46. J.J. Lee, F.T. Schmitt, R.G. Moore, S. Johnston, Y.T. Cui, W. Li, Z.K. Liu, M. Hashimoto, Y. Zhang, D.H. Lu, T.P. Devereaux, D.H. Lee, and Z.X. Shen, *Nature* **515**, 245 (2014).

47. Lin Zhao, Aiji Liang, Dongna Yuan, Yong Hu, Defa Liu, Jianwei Huang, Shaolong He, Bing Shen, Yu Xu, Xu Liu, Li Yu, Guodong Liu, Huaxue Zhou, Yulong Huang, Xiaoli Dong, Fang Zhou, Zhongxian Zhao, Chuangtian Chen, Zuyan Xu, and X.J. Zhou, *Nature Commun.* **7**, 10608 (2016).

48. Han Fu, K.V. Reich, and B.I. Shklovskii, *Zh. Eksp. Teor. Fiz.* **130**, 530 (2016) [*JETP* **122**, No. 3 (2016)].

49. Yuanjun Zhou and A.J. Mills, *ArXiv:1603.02728*.

50. M.X. Chen, D.F. Agterberg, and M. Weinert, *ArXiv:1603.03841*.

51. L.P. Gor'kov, *Phys. Rev. B* **93**, 060507 (2016).

52. P. Nozieres and S. Schmitt-Rink, *J. Low Temp. Phys.* **59**, 195 (1985).

53. M. Randeria, in: *Bose-Einstein Condensation*, A. Griffin, D.W. Snoke, and S. Stringari (eds.), Cambridge University Press (1995), p. 355.